Interaction between calcium-free calmodulin and IQ motif of neurogranin studied by nuclear magnetic resonance spectroscopy

ARTICLE *in* ANALYTICAL BIOCHEMISTRY · MAY 2003

Impact Factor: 2.22 · DOI: 10.1016/S0003-2697(03)00007-1 · Source: PubMed

ACADEMIC PRESS

Available online at www.sciencedirect.com

SCIENCE DIRECT®

Analytical Biochemistry 315 (2003) 175–182

ANALYTICAL BIOCHEMISTRY

www.elsevier.com/locate/yabio

Interaction between calcium-free calmodulin and IQ motif of neurogranin studied by nuclear magnetic resonance spectroscopy

Yanfang Cui,[a,c,*,1] Jian Wen,[b,1] Kong Hung Sze,[b] David Man,[b] Donghai Lin,[b] Maili Liu,[a] and Guang Zhu[b,2]

[a] *State Key Laboratory of Magnetic Resonance and Atomic and Molecular Physics, Wuhan Institute of Physics and Mathematics, The Chinese Academy of Sciences, Wuhan 430071, People's Republic of China*

[b] *Department of Biochemistry, The Hong Kong University of Science and Technology, Kowloon, Hong Kong*

[c] *Department of Chemistry, Central China Normal University, Wuhan 430079, People's Republic of China*

Received 24 July 2002

Abstract

The interaction of Ca^{2+}-free calmodulin (apoCaM) with the IQ motif corresponding to the calmodulin-binding domain of neurogranin has been studied by nuclear magnetic resonance (NMR) methods. The NMR spectra of uncomplexed apoCaM and apoCaM in complex with the IQ motif recorded at 750 MHz were studied and the backbone assignments of the protein in both forms were obtained by triple-resonance multidimensional NMR experiments. Chemical shift perturbations were used to map the binding surfaces. Only a single set of resonances was observed throughout the titration, indicating that the binding interaction is under fast exchange. Analysis of chemical shift changes indicates that (a) the main interaction and conformational changes occur in the C-terminal domain of calmodulin and (b) linker-1 (residues 40–44) between EF-1 and EF-2, linker-3 (residues 112–117) between EF-3 and EF-4, and the end of the α-helix H (residues 145–148) may be involved in the binding process. The dissociation constant (K_d), estimated by fitting the chemical shift changes against the IQ peptide concentration, ranged from about 1.2×10^{-5} to 8.8×10^{-5} M. This result demonstrates that the interaction falls into the weak binding regime.

Keywords: Ca^{2+}-free calmodulin (apoCaM); IQ motif; Neurogranin; Dissociation constant (K_d); Binding; Nuclear magnetic resonance (NMR)

Calmodulin (CaM),[3] a 148-residue protein (M_r 16.7 kDa) found in all eukaryotic cells, has been extensively studied as a primary Ca^{2+}-binding protein [1–6]. CaM couples the intracellular Ca^{2+} signal to many essential cellular events by binding and regulating the activities of more than 40 different proteins and enzymes. In particular, Ca^{2+}-free CaM (apoCaM) binds to a variety of proteins whose target sequences are very restricted. Proteins such as unconventional myosins, neuromodulin, and neurogranin (Ng) bind with CaM at low Ca^{2+} concentrations, and functional changes are triggered at higher levels of Ca^{2+} [7,8]. All such targets are characterized by a special sequence of about 25 residues called the "IQ motif," its core consensus sequence has the form IQXXXRGXXXR (X is an any amino acid) [9]. As far as we know, the binding of apoCaM with the IQ motif has not been extensively studied. Until now, only a theoretical model [10] had been developed by comparing the high similarity of CaM with essential light chains; this model addressed how apoCaM binds to the IQ motif of unconventional brush border myosin I.

Neurogranin, also known as RC3 [11] and p17 [12], consisting of 78 amino acids, is a neural-specific, calmodulin-binding protein that is phosphorylated at serine 36 by protein kinase C within its IQ domain in the core sequence IQASFRGHMAR. Ng plays important

* Corresponding author. Fax: +86-27-87885291.

E-mail addresses: yfcui@wipm.ac.cn (Y. Cui), gzhu@ust.hk (G. Zhu).

[1] These two authors contributed equally to this work.

[2] Also corresponding author.

[3] *Abbreviations used:* CaM, calmodulin; apoCaM, Ca^{2+}-free calmodulin; Ng, neurogranin; 3D, three-dimensional; 2D, two-dimensional.

0003-2697/03/$ - see front matter © 2003 Elsevier Science (USA). All rights reserved.
doi:10.1016/S0003-2697(03)00007-1

roles in controlling a variety of physiological processes, including tumor promotion, signal transduction, exocytosis, and gene expression [13]. The 3D structure of neurogranin is not yet available. When Ca^{2+} is absent or its concentration is very low, the IQ domain of Ng will bind to CaM in a dephosphorylated form and separate with CaM as the concentration of Ca^{2+} increases. The complex structure of apoCaM binding to Ng has also not been described to date. To understand the binding process of apoCaM with Ng, a special IQ motif peptide based on the calmodulin-binding domain sequence of bovine neurogranin was used in this study. Chemical shift perturbations were monitored by recording 2D ^{1}H-^{15}N HSQC spectra of $^{15}N/^{13}C$-labeled apoCaM when the unlabeled IQ motif peptide was titrated into the protein solution.

Chemical shift perturbation is extremely sensitive to molecular interactions and has been widely used to map binding surfaces [14,15]. When a protein interacts with a ligand, changes in the environments of the nuclei at the binding sites will inevitably cause changes in the chemical shifts. Conformational changes due to the interaction will result in additional chemical shift perturbations beyond the direct binding interaction. Therefore, chemical shift perturbation has been regarded as an excellent indicator of allosteric processes [16]. Since chemical shift perturbation is sensitive to specific interactions over a wide range of affinities (K_d ranges from 10^{-4} to 10^{-9} M), it has been successfully used in drug screening to identify molecules that bind to a protein target [17,18]. This method is well suited to a binding study of apoCaM complexed with the IQ motif because the system has been demonstrated to be a weak binding system through lineshape analysis after the titration experiments.

The magnitude of the dissociation constant, K_d, has an important effect on many NMR parameters and plays a significant role in determining the kind of information that can be obtained for a particular protein–ligand interaction. In general, an interaction is referred to as tight binding for $K_d < 10^{-8}$ M, as intermediate binding for K_d between 10^{-6} and 10^{-8} M, and as weak binding for $K_d > 10^{-5}$ M. When a particular protein–ligand interaction is indicated as a first-order fast-exchange process, the observed NMR parameters including the chemical shifts, spin–lattice relaxation rates, spin–spin relaxation rates (or linewidths), and diffusion coefficients of the bound protein or ligand can be cast into weighted averages of the free and bound forms [19]. In principle, the values of the observed parameters as a function of the varied protein or ligand concentration can be used to derive the K_d. Recently, with the introduction of affinity NMR [20] for characterizing protein–ligand interactions and SAR-NMR [17] for discovering high-affinity ligands, NMR-based diffusion coefficient measurements have found applicability in the determination of the protein–ligand dissociation constants [21,22]. Chemical shifts and relaxation rates have long been used to derive K_d. Most recently, transverse and/or selective longitudinal relaxation parameters in combination with competition binding experiments were exploited in extracting an approximate value of K_d and then detecting high-affinity ligands that bind covalently to the receptor [23]. In this study we carried out binding analysis of apoCaM with the IQ motif peptide. We not only derived the K_d value for the binding process but also mapped the binding site information from the chemical shift changes of apoCaM upon binding with the IQ peptide. We did not utilize diffusion coefficients and relaxation rate measurements to derive K_d, because the quite long correlation time of the protein may cause errors in diffusion coefficients and relaxation rate measurements when a protein of the size of calmodulin rather than a small ligand is monitored.

Materials and methods

Preparation of NMR samples

Uniform labeling of apoCaM with ^{15}N and ^{13}C was accomplished by growing CaM-expressing *Escherichia coli* JM105 in M9 minimal media containing 1 g/L ^{13}C–glucose and 1 g/L $^{15}NH_4Cl$ as sources of nitrogen and carbon. When the OD reached 0.6, isopropyl β-D-thiogalactoside was added to 2 mM, and expression was induced for 6–8 h at 37 °C. The cells were harvested by centrifugation and then resuspended. Lysozyme was added to 200 μg/ml, and the suspension was incubated at 4 °C for 1 h. $MgCl_2$ and DNase were added to concentrations of 10 mM and 10 μg/ml, respectively. The lysate was incubated for another 2 h. After centrifugation and filtration, the mixture was loaded to a phenyl–Sepharose column to be equilibrated. The apoCaM was eluted and then dialyzed against distilled water. The final apoCaM protein was dissolved for NMR experiments in a buffer consisting of 20 mM K_2HPO_4, 4 mM dithiothreitol, and 5 mM EDTA at pH 7.5 in 90% H_2O/10% D_2O. Under this carefully selected sample condition, the protein can reach the high solubility necessary for NMR experiments, and can exist in its native structure although the ionic strength used here was short of the 0.15 M associated with physiological conditions. The final protein concentration of 1 mM was determined both by the Coomassie plus protein assay (Pierce) and by SDS–PAGE.

The peptide used was based on the sequence of bovine neurogranin with the sequence of ANAAAAKIQASFRGHMARKKIKSG. It was prepared commercially (New England Peptide Inc.). The peptide was purified by HPLC and identified by matrix-assisted laser desorption ionization-time of flight DE mass spectrometry.

NMR spectroscopy

All NMR experiments were performed at 30 °C on a four-channel Varian Unity INOVA 750-MHz spectrometer with z-axis pulsed-field gradient capabilities. The employed parameters of the experiments are shown in Table 1. The spin-locking time for 3D TOCSY-HSQC was 70 ms and the mixing times for 3D NOESY-HSQC were 50, 70, and 100 ms. Quadrature detections in the F_1 dimension were achieved using the states-TPPI approach. Data were processed using the nmrPipe [24] software. Linear prediction [25] in the indirect dimensions and zero-filling in all dimensions were used before the Fourier transformation. ^{1}H, ^{13}C, and ^{15}N chemical shifts were referenced to DSS [26]. All the NMR methods employed can be found in the book edited by Cavanagh et al. [27].

Titration of apoCaM with the IQ peptide

We sought to reach an ultimate IQ peptide concentration of about 4 mM after the titration. We thus dissolved 6.46 mg of the IQ motif peptide (M_r 2.86 kDa) in distilled water and prepared a 64 µl stock solution. The IQ peptide concentration in the stock solution was 35.25 mM. We divided the 64 µl of stock solution of the peptide into 16 aliquots. Each aliquot was 4 µl. All 16 aliquots of the peptide were added stepwise into a $^{13}C/^{15}N$-labeled apoCaM sample (with an initial concentration of 1 mM and an initial volume of 0.5 ml). At each titration point, a 2D ^{1}H-^{15}N HSQC spectrum was recorded for apoCaM after 10 min of equilibration. Only 7 titration points from the total of 17 were chosen for the chemical shift data-fitting to obtain the K_d values, since peaks in some spectra overlapped. Practically, after the 12th titration point, there were no more observable chemical shift changes. The concentrations of the IQ peptide (C_{IQ}) at the 7 chosen titration points were 0, 0.28, 0.83, 1.09, 2.12, 2.61, and 2.85, corresponding to titration with 0, 1, 3, 4, 8, 10, and 11 aliquots of the IQ peptide, respectively. The corresponding concentrations of apoCaM protein (C_{apoCaM}) were 1.00, 0.99, 0.98, 0.97, 0.94, 0.93, and 0.92, respectively.

Results and discussion

Resonance assignments

For uncomplexed apoCaM and complexed apoCaM, 144 of 148 backbone resonances (148 residues minus 2 prolines and the first 2 residues) were unambiguously assigned. The assignments are labeled on the 2D ^{1}H-^{15}N HSQC spectra of uncomplexed apoCaM and the complexed apoCaM shown in Figs. 1 and 2, respectively. The backbone sequential resonance assignments for uncomplexed apoCaM were first achieved using the experiments listed in Table 1. The sequential connectivities were determined using TOCSY-HSQC, NOESY-HSQC, HNCACB, and HN(CO)CACB experiments and were further confirmed using HNCA and HN(CO)CA experiments. The backbone assignment of the complexed apoCaM was more complicated than originally expected. Only part of the assignment could be obtained by following up the chemical shift changes that occurred during the titration with the IQ peptide. Since the overlap in the spectra of the complex was more serious (Fig. 2) than that of the uncomplexed protein (Fig. 1), TOCSY-HSQC, NOESY-HSQC, HNCACB, and HN(CO)CACB spectra of the complexed apoCaM were therefore also utilized to assist the assignment of the complexed apoCaM. Moreover, some peaks from residues in the C terminus were too weak to be observable in these 3D spectra, which made it necessary to record the more sensitive HNCO, HNCA, and HN(CO)CA spectra for the assignment of complexed apoCaM.

Chemical shift perturbations of apoCaM upon binding with the IQ motif

Specific chemical shift perturbations were observed in the 2D ^{1}H-^{15}N HSQC spectra of apoCaM upon binding with the IQ peptide. Fig. 3 shows the chemical shift perturbations of some typical peaks during the titration. At the first few titration points, the chemical shifts change significantly. Only one set of resonances was

Table 1
Summary description of heteronuclear NMR experiments used for the sequential assignments for uncomplexed apoCaM and complexed apoCaM binding with the IQ peptide

Experiments	Acquired data (complex points)			Spectral widths (Hz)		
	F_1	F_2	F_3	ω_1	ω_2	ω_3
^{15}N-HSQC	1024(H)	128(N)	—	10473	1850	—
^{15}N-TOCSY-HSQC	512(H)	90(H)	36(N)	6000	5600	1200
^{15}N-NOESY-HSQC	512(H)	90(H)	37(N)	6000	5600	1200
HNCACB	512(H)	56(C)	35(N)	9476	12000	1850
HN(CO)CACB	512(H)	56(C)	35(N)	9476	12000	1850
HNCO	512(H)	34(C)	34(N)	9476	3017	1850
HNCA	512(H)	34(C)	34(N)	9476	3017	1850
HN(CO)CA	512(H)	34(C)	24(N)	9476	3017	1850

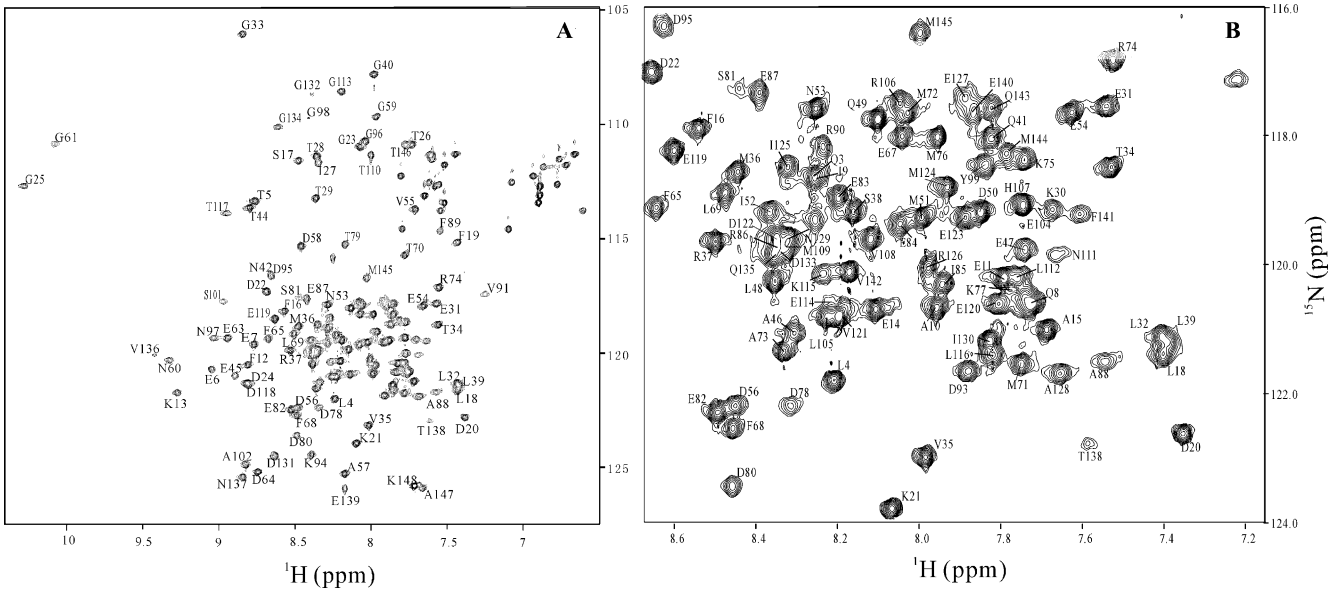

Fig. 1. 2D ^{1}H-^{15}N HSQC spectrum of ^{15}N/^{13}C-labeled apoCaM obtained at 30 °C and pH 7.5. The most crowded region in (A) is expanded in (B).

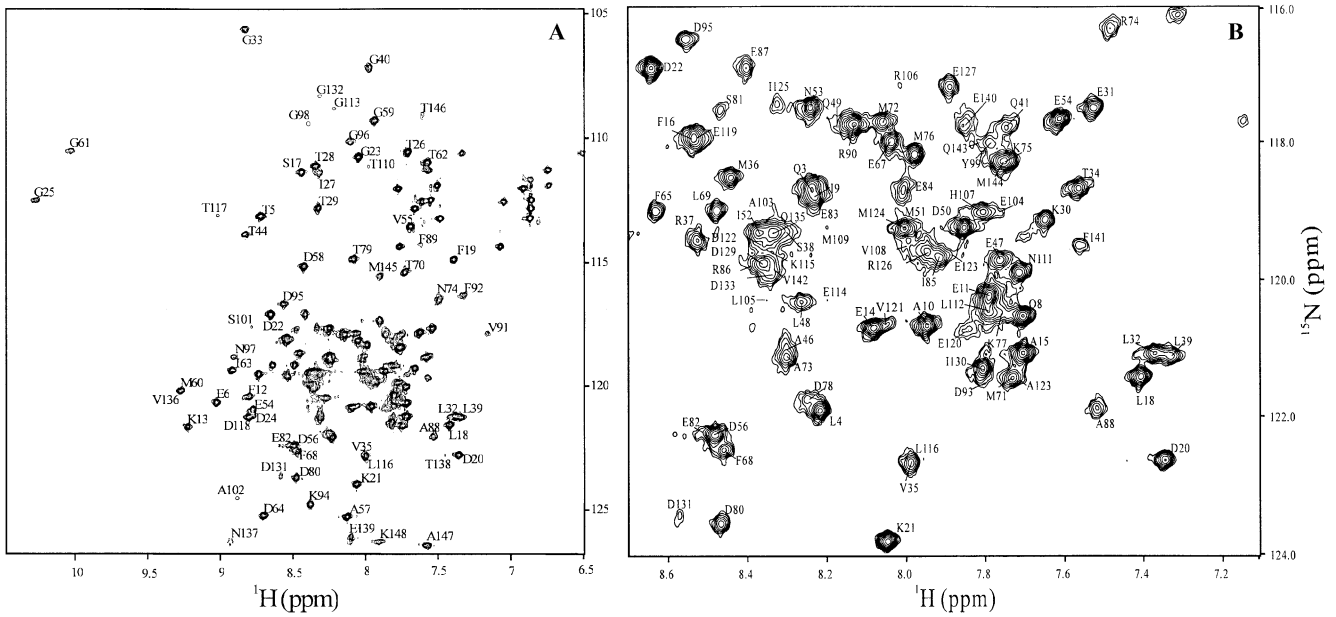

Fig. 2. 2D ^{1}H-^{15}N HSQC spectrum of ^{15}N/^{13}C-labeled apoCaM in complex with the IQ peptide at a molar ratio of apoCaM to the IQ motif of 0.32:1 obtained at 30 °C and pH 7.5. The most crowded region in (A) is expanded in (B).

observed throughout the titration, which indicates that the binding of apoCaM to the IQ peptide is a first-order exchange process and falls into the fast-exchange regime. Therefore, we suppose that the interaction is most likely a weak binding. This supposition will be confirmed by the calculated dissociation constant (see next subsection).

apoCaM has two similar domains. Each domain, consists of a pair of helix–loop–helix motifs which are commonly called the EF-hands [1]. The ''loops'' of the two EF-hands in each domain are linked by a short antiparallel β-sheet. Ca^{2+}-saturated CaM structures [2,3] reveal that the protein has a dumbbell shape comprising the N-terminal and C-terminal domains connected by a long central solvent-exposed α-helix (residues 77–81), the so-called ''central helix.'' NMR studies of apoCaM also show that both lobes adopt ''closed'' and ''almost closed'' conformations [4,5]. It has been demonstrated by NMR that, upon binding to target peptides, the flexible ''central helix'' linker is further extended, which allows CaM to accommodate targets of different sizes [6].

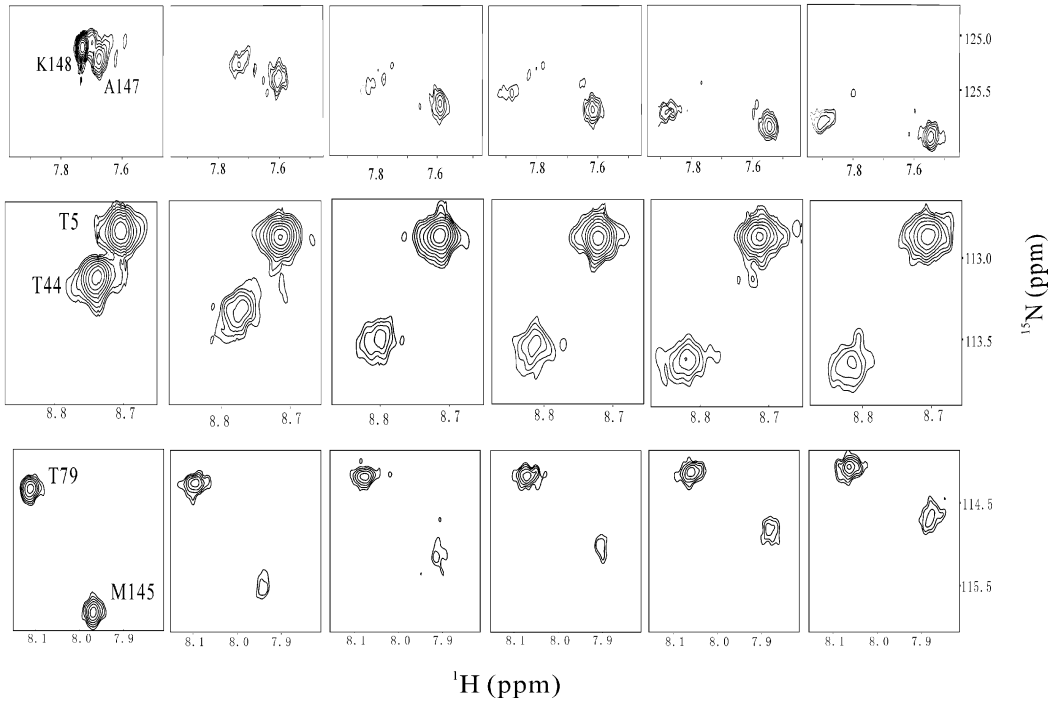

Fig. 3. Chemical shift perturbations of some typical peaks of apoCaM during the titration with the IQ peptide. From left to right, the molar ratio of apoCaM to the IQ peptide is 4:0, 3.54:1, 1.18:1, 0.89:1, 0.44:1, and 0.30:1, respectively.

Chemical shift changes between uncomplexed apoCaM and saturated apoCaM in complex with the IQ peptide versus the residue numbers of the protein are shown in Fig. 4. In the N-terminal domain, significant chemical shift perturbations were observed only in residues 34–49. These residues are located at a segment extending from the middle of the α-helix B (residues 32–38) to the beginning of the α-helix C (residues 45–55). In the C-terminal domain, significant chemical shift perturbations occur in three regions of the sequentially connected residues 102–107, 111–118, and 145–148. The largest chemical shift changes occurred at residue L116. This residue and the two sequentially connected residues, K115 and T117, are in the middle of the linker. A similar situation occurred in the residues 40–44 and 101–105, which are located in a β-sheet in the C-terminal domain. The end of the last α-helix (residues 145–148) also shows significant chemical shift perturbations, indicating that this helix may also interact with the peptide.

Those residues that experienced overall chemical shift perturbations larger than 0.1 ppm are mapped in red in the CPK surface-style diagram of the uncomplexed apoCaM structure shown in Fig. 5. The diagram exhibits the main chemical shift change regions of apoCaM upon binding with the IQ motif peptide. These regions contain mostly hydrophobic and polar residues and may be involved in hydrophobic interactions and hydrogen bonding with the IQ peptide, thus contributing to the specificity of the interaction. Additionally, local conformational changes due to the IQ peptide binding may also contribute to the specific chemical shift changes of some residues. The binding or conformational changes mainly occurred in the C-terminal domain of apoCaM. This experimental result fits the prediction of the theoretical model [10], which proposed that the interactions mainly occur at the C-terminal domain of apoCaM and that the IQ motif binds less tightly at the N-terminal domain of apoCaM.

Equilibrium dissociation constant of apoCaM binding to the IQ motif

As the above titration experiments have shown, some of the resolved resonances in the 2D ^{1}H-^{15}N HSQC spectra shifted progressively (Fig. 3), and no extra peaks appeared during the titration. These facts imply that the IQ motif binds to apoCaM with relatively low affinity and that the bound form and the free form of apoCaM are in fast chemical exchange on the NMR time scale (millisecond to second) [28]. That means that the lifetime of the apoCaM · IQ complex is short compared with $(\delta_b - \delta_f)^{-1}$, given that a nucleus of the protein has chemical shifts of δ_b and δ_f in the bound and free forms, respectively. Under this condition, the observed single set of resonances is the population-weighted average of the chemical shifts of the free and bound forms [29],

$$\delta_{obs} = \delta_b X_b + \delta_f X_f, \quad (1)$$

where δ_{obs} is the observed chemical shift of the nucleus of the protein, and X_b and X_f are the molar fraction of

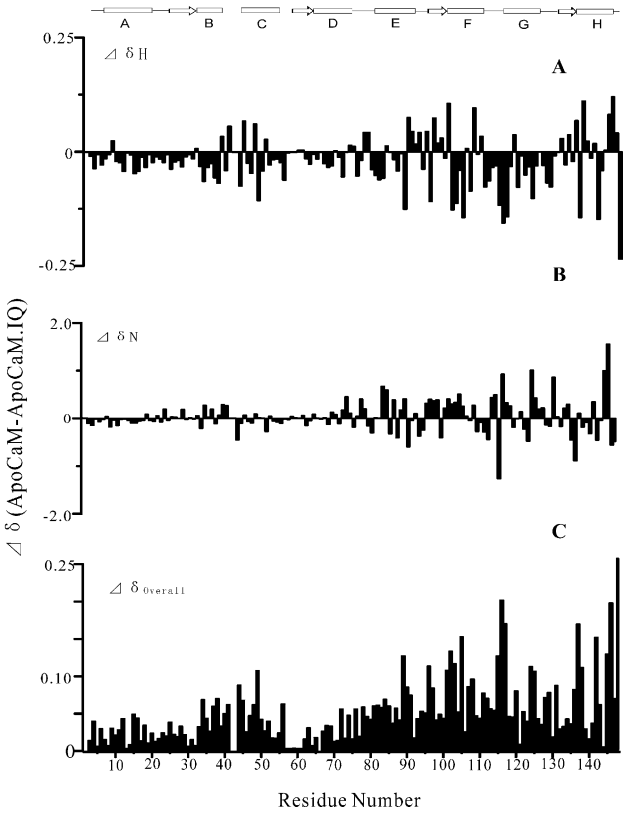

Fig. 4. Chemical shift changes between uncomplexed apoCaM and saturated apoCaM in complex with the IQ peptide. Shown are the chemical shift changes experienced by backbone amide proton, $\Delta\delta$H (A), amide nitrogen, $\Delta\delta$N (B), and overall $\delta_{overall}$ ($\delta_{overall} = \sqrt{(\Delta H)^2 + (\Delta N \gamma_N/\gamma_H)^2}$; γ is the gyromagnetic ratio of a nucleus) (C). Large perturbations are observed for residues T44, Q49, F89, A102, L105, K115, L116, T117, M124, N137, V142, M145, T146, and K148.

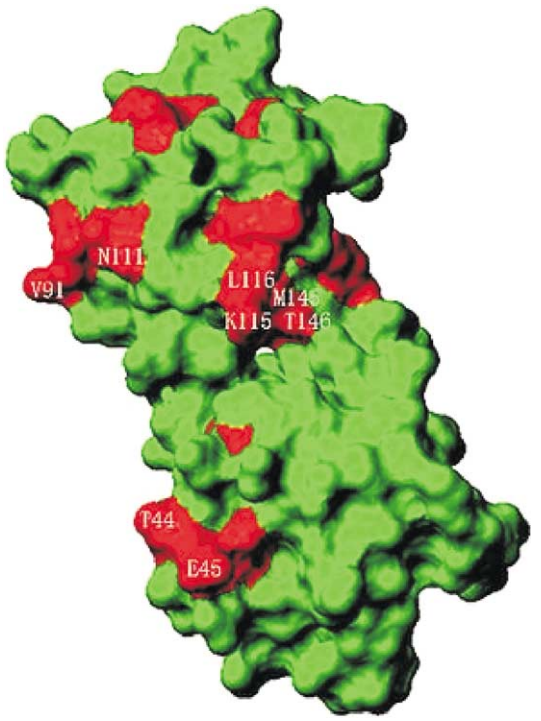

Fig. 5. CPK surface-style diagram of apoCaM structure showing the chemical shift perturbations of apoCaM molecule upon binding with the IQ motif. All residues in the diagram are colored in green in original and those residues that experienced overall chemical shift perturbations larger than 0.1 ppm are further mapped in red.

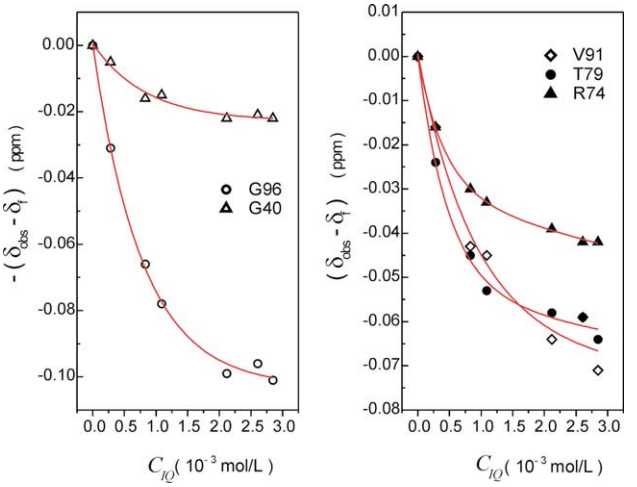

Fig. 6. Difference between the observed backbone amide proton chemical shift of the complexed apoCaM and that of the uncomplexed apoCaM, $(\delta_{obs} - \delta_f)$ for the residues shifted to lower frequency and $-(\delta_{obs} - \delta_f)$ for those shifted to higher frequency, as a function of the IQ motif concentration (C_{IQ}). The curves are the second-order exponential decay fits to the data.

the bound and free forms of the protein, respectively. To characterize quantitatively the interaction between the apoCaM and the IQ peptide in greater detail, we calculated the equilibrium dissociation constant, K_d, of apoCaM binding with the IQ peptide from the chemical shift changes of apoCaM during the stepwise titration.

It is generally considered that the specific binding of a ligand to a protein conforms to the stoichiometric relationship according to the site-binding model. The binding of the reversible ligand, IQ, to the protein, apoCaM, results in the formation of a noncovalently bound complex, apoCaM · IQ, represented by the equilibrium

$$\text{apoCaM} + \text{IQ} \underset{k_{-1}}{\overset{k_{+1}}{\rightleftharpoons}} \text{apoCaM} \cdot \text{IQ}.$$

Then, the equilibrium dissociation constant, K_d, is given by

$$K_d = \frac{[apoCaM][IQ]}{[apoCaM \cdot IQ]} = \frac{k_{-1}}{k_{+1}}, \qquad (2)$$

where $[apoCaM]$ and $[IQ]$ are the equilibrium concentrations of the free protein and the ligand peptide, respectively, and $[apoCaM \cdot IQ]$ is the equilibrium concentration of the complex. From Eqs. (1) and (2), and the requirements of mass conservation, the final relationship between the observed chemical shifts of

Table 2
Calculated K_d ($\times 10^{-5}$ M) of the binding interaction between apoCaM and IQ peptide

Residue No.	K_d	Residue No.	K_d	Residue No.	K_d
T34	6.56	T79	7.63	G96	7.02
G40	1.32	E87	1.23	N111	2.35
T44	5.58	F89	4.75	K115	2.03
E47	7.71	K94	5.20	L116	1.86
R74	8.82	D95	6.47	T117	2.34

Listed values for the typical residues of the protein are the fitting results from the chemical shift perturbations experienced by the backbone amide protons ($\Delta\delta$H) versus the peptide concentrations; standard deviations for K_d in the simulation are about ± 0.03 ($\times 10^{-5}$ M).

apoCaM, δ_{obs}, with the varied concentration of the ligand IQ motif, C_{IQ}, is given by [29]

$$\delta_{obs}-\delta_f=(\delta_b-\delta_f)\left\{(C_{apoCaM}+C_{IQ}+K_d)-\sqrt{(C_{apoCaM}+C_{IQ}+K_d)^2-4C_{apoCaM}C_{IQ}}\right\}/2C_{IQ}, \quad (3)$$

where C_{apoCaM} and C_{IQ} are the total concentration of the protein and the ligand, respectively. Since the C_{apoCaM} and δ_f are exactly known from the titration experiments, fitting Eq. (3) to the data as a plot of δ_{obs} versus C_{IQ} yields the values of K_d and δ_b using regression simulation. In this work, the data-fitting was performed using an in-house nonlinear regression AWK [30] program. The chemical shifts of backbone amide proton ($\Delta\delta$H), the amide nitrogen ($\Delta\delta$N), and the overall ($\Delta\delta_{overall}$) as shown in Fig. 4 were fitted separately. Some typical peaks that were well resolved and had large chemical shift perturbations were used to estimate the K_d values. Fig. 6 shows the plots of the backbone amide proton chemical shift differences between δ_{obs} and δ_f for a few typical residues versus the IQ peptide concentrations; the second-order exponential fitting curves are also shown. In this figure, the chemical shift changes are denoted by $(\delta_{obs}-\delta_f)$ for the residues that shifted to higher frequency and by $(\delta_{obs}-\delta_f)$ for those that shifted to lower frequency. Though the residues at the far end of the C terminus such as R148 and R147 experienced the largest shifts, they were not used to calculate K_d because of the consideration that their flexible motion effect may cause overestimation. The simulated K_d had values ranging from 1.2×10^{-5} to 8.8×10^{-5} M (Table 2). This result confirmed that the interaction between apoCaM and IQ motif of Ng falls into the weak binding category. Because of the weak binding, at least a 2:1 molar ratio of the IQ peptide to apoCaM is required to have over 90% apoCaM · IQ in the complex form.

Conclusions

From the chemical shift perturbation analysis of the binding of apoCaM with the IQ motif of Ng, we have shown that the main interaction and conformation changes likely occur in the C-terminal domain of apoCaM. Compared with the prediction of the theoretical model [10], we proposed in more detail that linker-1 between EF-1 and EF-2 (residues 40–44), linker-3 between EF-3 and EF-4 (residues 112–117), and the end of the last α-helix are possibly involved in the binding of apoCaM with the IQ motif of Ng. The calculated K_d of the interaction has an order of magnitude of 10^{-5} M, which demonstrates that the interaction between apoCaM and IQ motif of Ng is a typical weak binding interaction. As the IQ motif is the binding domain of Ng, one can expect that Ng may also weakly bind to apoCaM. Weak binding makes it easy for Ng to constantly bind/separate with apoCaM in the absence/presence of Ca^{2+}. Together with the knowledge that the center part of Ng (residues 28–33) has strong helical propensity in the presence of sodium dodecyl sulfate micelle [31], the binding mechanism of Ng with apoCaM can be outlined. This may help the determination of the still unknown complex structure of apoCaM binding with Ng. Furthermore, as several target proteins that can bind to CaM are characterized by a similar special IQ motif, the NMR analysis of the binding of apoCaM with the IQ motif of Ng may also contribute to the understanding of the binding of CaM with other target proteins.

Acknowledgments

This work was performed in the Center of Biological NMR, the Hong Kong University of Science and Technology and was supported in part by grants to G.Z. from the Research Grants Council of Hong Kong (6199/99M and 6208/00M) and to D.L. from the National Natural Science Foundation of China (19975038).

References

[1] S. Nakayama, R.H. Kretsinger, Evolution of the EF-hand family of proteins, Annu. Rev. Biophys. Biomol. Struct. 23 (1994) 473–507.
[2] Y.S. Babu, J.S. Sack, T.J. Greenhough, C.E. Bugg, A.R. Means, J. Cook, Three-dimensional structure of calmodulin, Nature 315 (1985) 37–40.
[3] R.H. Kretsinger, S.E. Rudnick, L.J. Weissman, Crystal structure of calmodulin, J. Inorg. Biochem. 28 (1986) 289–302.

[4] M. Zhang, T. Tanaka, M. Ikura, Calcium-induced conformational transition revealed by the solution structure of apo calmodulin, Nat. Struct. Biol. 2 (1995) 758–767.
[5] H. Kuboniwa, N. Tjandra, S. Grzesiek, H. Ren, C.B. Klee, A. Bax, Solution structure of calcium-free calmodulin, Nat. Struct. Biol. 2 (1995) 768–777.
[6] M. Ikura, G.M. Clore, A.M. Gronenborn, G. Zhu, C.B. Klee, A. Bax, Solution structure of a calmodulin-target peptide complex by multidimensional NMR, Science 256 (1992) 632–638.
[7] J.S. Wolenski, Regulation of calmodulin-binding myosins, Trends Cell Biol. 5 (1995) 310–316.
[8] E.R. Chapman, D. Au, K.A. Alexander, T.A. Nicolson, D.R. Storm, Characterization of the calmodulin binding domain of neuromodulin. Functional significance of serine 41 and phenylalanine 42, J. Biol. Chem. 266 (1991) 207–213.
[9] A. Houdusse, C. Cohen, Structure of the regulatory domain of scallop myosin at 2 Å resolution: implications for regulation, Structure 4 (1996) 21–32.
[10] A. Houdusse, M. Silver, C. Cohen, A model of Ca(2+)-free calmodulin binding to unconventional myosins reveals how calmodulin acts as a regulatory switch, Structure 9 (1996) 1475–1490.
[11] J.B. Watson, E.F. Battenberg, K.K. Wong, F. Bloom, J.G. Sutcliffe, Subtractive cDNA cloning of RC3, a rodent cortex-enriched mRNA encoding a novel 78 residue protein, J. Neurosci. Res. 26 (1990) 397–408.
[12] J. Baudier, C. Bronner, D. Kligman, R.D. Cole, Protein kinase C substrates from bovine brain. Purification and characterization of neuromodulin, a neuron-specific calmodulin-binding protein, J. Biol. Chem. 264 (1989) 1824–1828.
[13] Y. Nishizuka, The molecular heterogeneity of protein kinase C and its implications for cellular regulation, Nature 334 (1988) 661–665.
[14] M. Pelleccia, S.Y. Stevens, K.C.W. Vander, D.H. Montgomery, E.H. Feng, L.M. Gierasch, E.R.P. Zuiderweg, Structural insights into substrate binding by the molecular chaperone DnaK, Nat. Struct. Biol. 7 (2000) 298–303.
[15] S.Y. Stevens, S. Sanker, C. Kent, E.R.P. Zuiderweg, Delineation of the allosteric mechanism of a cytidylyltransferase exhibiting negative cooperativity, Nat. Struct. Biol. 8 (2001) 947–952.
[16] N.A. van Nuland, G.J. Kroon, K. Dijkstra, G.K. Wolters, R.M. Scheek, G.T. Robillard, The NMR determination of the IIA(mtl) binding site on HPr of the Escherichia coli phosphoenol pyruvate-dependent phosphotransferase system, FEBS Lett. 315 (1993) 11–15.
[17] S.B. Shuker, P.J. Hajduk, R.P. Meadows, S.W. Fesik, Discovering high-affinity ligands for proteins-SAR by NMR, Science 274 (1996) 1531–1534.
[18] J. Weigelt, M. van Donggen, J. Uppenberg, J. Schultz, M. Wikström, Site-selective screening by NMR spectroscopy with labeled amino acid pairs, J. Am. Chem. Soc. 124 (2002) 2446–2447.
[19] D.K. Chang, W.J. Chien, A.I. Arunkumar, Conformation of a protein kinase C substrate NG (28-43), and its analog in aqueous and sodium dodecyl sulfate micelle solutions, Biophys. J. 72 (1997) 554–566.
[20] A. Chen, M.J. Shapiro, Affinity NMR, Anal. Chem. 72 (1999) 669–675.
[21] T.S. Derrick, E.F. McCord, C.K. Larive, Analysis of protein/ligand interaction with NMR diffusion measurements: the importance of eliminating the protein background, J. Magn. Reson. 155 (2002) 217–225, doi: 10. 1006/jmre. 2002. 2513.
[22] M. Liu, J.K. Nicholson, J.C. Lindon, Analysis of drug-protein binding using nuclear magnetic resonance based molecular diffusion measurements, Anal. Commun. 34 (1997) 225–228.
[23] C. Dalvit, M. Flocco, S. Knapp, M. Mostardini, R. Perego, B.J. Stockman, M. Veronesi, M. Varasi, High-throughput NMR-based screening with competition binding experiments, J. Am. Chem. Soc. 124 (2002) 7702–7709, doi: 10. 1021/ja020174b.
[24] F. Delaglio, S. Grzesiek, G.W. Vuister, G. Zhu, J. Pfeifer, A. Bax, NMRPipe: a multidimensional spectral processing system based on UNIX pipes, J. Biomol. NMR 6 (1995) 277–293.
[25] G. Zhu, A. Bax, Improved linear prediction of damped NMR signals using modified ''farword-backward'' linear prediction, J. Magn. Reson. 100 (1992) 202–207.
[26] D.S. Wishart, C.G. Bigam, J. Yao, F. Abildgaard, H.J. Dyson, E. Oldfield, J.L. Markley, B.D. Sykes, 1H, 13C and 15N chemical shift referencing in biomolecular NMR, J. Biomol. NMR 6 (1995) 135–140.
[27] J. Cavanagh, W.J. Fairbrother, A. Palmer III, N.J. Skelton, Protein NMR Spectroscopy: Principle and Practice, Academic Press, San Diego, 1995.
[28] G.M. Clore, A.M. Gronenborn, B. Birdsall, J. Feeney, G.C.K. Roberts, ^{19}F-n.m.r. studies of 3′,5′-difluoromethotrexate binding to *Lactobacillus casei* dihydrofolate reductase, Biochem. J . 217 (1984) 659–666.
[29] G.C.K. Roberts, in: NMR of Macromolecules: A Practical Approach, Oxford University Press, Oxford, 1993, pp. 164–166.
[30] A.J. Lennon, N.R. Scott, B.E. Chapman, P.W. Kuchel, Hemoglobin affinity for 2,3-bisphosphoglycerate in solutions and intact erythrocytes: studies using pulsed-field gradient nuclear magnetic resonance and Monte Carlo simulations, Biophys. J. 67 (1994) 2096–2109.
[31] A.V. Aho, B.W. Kernighan, P.J. Weinberger, The AWK programming language, Addison-Wesley Publishing Company, 1988.